Pitch and roll control mechanism for a hovering flapping wing MAV

M. Karásek,* A. Hua, Y. Nan, M. Lalami, and A. Preumont
Université libre de Bruxelles, Belgium

ABSTRACT

Hovering flapping flight is inherently unstable and needs to be stabilized actively. We present a control mechanism that modulates independently the wing flapping amplitude and offset by displacing joints of a flapping linkage mechanism. We demonstrate its performance by high speed camera recordings of the wing motion as well as by direct measurements of pitch moment and lift force. While flapping at 17 Hz the prototype produces 90 mN of lift and generates pitch moments from -0.7 N.mm to 1.1 N.mm. The mechanism shows low level of cross-coupling in combined pitch and roll commands.

1 INTRODUCTION

Flapping wing Micro Air Vehicles (MAVs) take the inspiration from nature. They mimic insects and hummingbirds who, unlike other larger birds, flap their wings in approximately horizontal plane, which allows them to hover for extended periods of time. Since the flapping flight of two winged animals is inherently unstable [1, 2, 3, 4], the animals stabilize their attitude by small changes of the wing angle of attack, of mean wing position and of flapping amplitude [5].

The stability can be augmented by an artificial increase of aerodynamic damping [6]. Passively stable MAVs use tails and sail-like damping surfaces [7, 8, 9], but stay sensitive to external disturbances. Tail-less flapping wing MAVs are unstable and, like their natural counterparts, need to be stabilized actively. Nevertheless, this also makes them very agile when manoeuvring. The active stabilization requires a feedback system that senses the changes in the MAV attitude and actively produces stabilizing moments around the pitch, roll and yaw axes.

Two strategies of moment generation were used in the existing MAVs. The Nano Hummingbird [10] generates the moments by three servos that modulate the wing twist, similar to the changes of angle of attack in insects. The second strategy, used by the Harvard robotic fly [11], generates the moments by modulating the wing flapping amplitude, mean position and difference of speed velocities in upstroke and downstroke. Two piezoactuators (PZTs) are used for propulsion and the control is implemented by shaping the driving signals for the PZTs.

*matej.karasek@ulb.ac.be, http://scmero.ulb.ac.be

In this paper we present a control mechanism based on flapping amplitude and offset (mean wing position) modulation, see Figure 1. A novel solution is used to modify the kinematics of the flapping linkage mechanism by displacing its joints by servo motors. We describe the concept kinematics and prototype design and present experimental results obtained by high speed camera and force balance measurements.

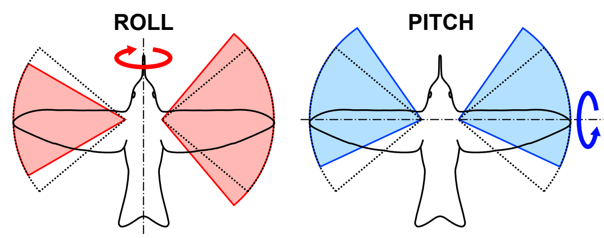

Figure 1: Control via flapping amplitude & offset modulation.

2 FLAPPING MECHANISM

The flapping mechanism was already presented in [12], see Figure 2. A linkage mechanism, driven by a DC motor, is used to transform the motor shaft rotation into the flapping motion of the wings. It has two stages: a slider crank based mechanism generates a low amplitude oscillating motion and a four-bar linkage amplifies the motion to the desired amplitude $\Phi = 120°$ (Figure 3). The slider crank mechanism is common for the two wings. The advantage of using two stages is that the asymmetries coming from individual stages can be compensated by an appropriate choice of dimensions.

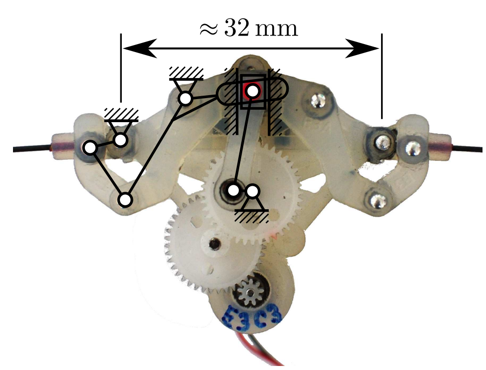

Figure 2: Flapping mechanism prototype and its kinematic representation.

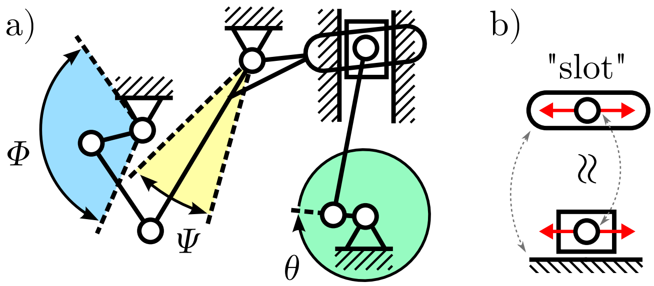

Figure 3: a) Two stages of the flapping mechanism: slider crank with a rocker producing oscillating motion and a four-bar mechanism for motion amplification. b) The symbol for a "slot" kinematic pair (equivalent to a slider).

2.1 Kinematics

The kinematics of the proposed mechanism can be treated separately for each mechanism stage. Using the notation of Figure 4 the kinematics of the first stage can be expressed analytically as

$$\psi = \arctan\left(\frac{A_1 - L_1\cos\theta - \sqrt{L_2^2 - L_1^2\sin^2\theta}}{L_3}\right) + \frac{\pi}{2} \tag{1}$$

where θ is the input angle and ψ is the angle of the intermediary link 3-4. The analytic solution of the second (amplification) stage is a classical solution of a four bar mechanism

$$\phi = \arctan\left(\frac{a}{b}\right) - \arccos\left(\frac{c}{\sqrt{a^2+b^2}}\right) \tag{2}$$

where

$$\begin{aligned} a &= -2L_4L_6\sin(\psi-\alpha) \\ b &= 2A_2L_6 - 2L_4L_6\cos(\psi-\alpha) \\ c &= L_5^2 - A_2 - L_4^2 - L_6^2 + 2A_2L_4\cos(\psi-\alpha) \end{aligned} \tag{3}$$

The dimensions were optimized numerically for the desired amplitude as well as for symmetry of upstroke and downstroke velocity profiles. The final dimensions in Table 1 result into nearly harmonic flapping motion. The final structure of the flapping mechanism was rearranged (compared to Figure 4) to minimize the overall mechanism dimensions. The mutual orientation of the two stages was adapted as in Figure 2 and the wing bar was connected to the output link at an angle in order to obtain symmetric motion with respect to the lateral body axis.

2.2 Mechanism design

The frame and the links of the flapping mechanism are all 3D printed by PolyJet technology in Digital ABS photopolymer. Thanks to very fine resolution (42 μ m in xy, 16 μ m in z - Objet Eden series) the parts do not require any further

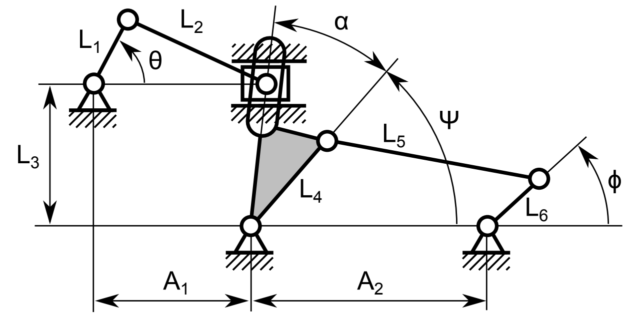

Figure 4: Kinematic scheme of the flapping mechanism.

Table 1: Mechanism dimensions (lengths in mm, angles in °)

L_1	L_2	L_3	L_4	L_5	L_6	A_1	A_2	α
2.25	12	8	14	7.53	3.57	11	-9.2	-70

processing. Aluminium and steel rivets are used to connect the links together. The shoulder hinges have integrated brass bearings to increase their robustness.

The motor is placed above the flapping mechanism, in the centre between the two wing shoulders. A two stage gearbox (reduction 1:19.75) is used to reduce the motor speed. The most recent version of the flapping mechanism weights 6.9 g without the motor. With a 5.2 g brush-less DC motor (Faulhaber 0824) and 90 mm wings it produces 155 mN ≈ 15.8 g lift force while flapping at 24 Hz. The electrical power consumption is 4W.

2.3 Wings

The design of the wings is inspired by the Nano Hummingbird [10]. The wing is made of a 15 micron thin polyester membrane. It has two sleeves, one on the leading edge and one on the root edge (close to the body), that accommodate the leading edge and root edge carbon-fibre-reinforced polymer (CFRP) bars. The sleeves can rotate freely around the bars and are reinforced with Icarex for durability. Since the angle between the sleeves is greater than the angle between the bars the wing becomes cambered and twisted after the assembly (Figure 5). The camber is bistable - it flips passively from one side to another depending on the direction of motion. The root bar is fixed directly to the frame

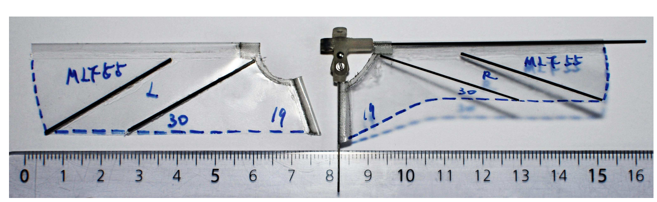

Figure 5: Polyester film wing becomes cambered after assembly.

and is aligned with the shoulder axis, the leading edge bar is connected to the output link of the flapping mechanism.

The wings are hand built - a reasonable accuracy and repeatability is achieved by printing the desired shape on a sheet of paper that is attached under the membrane and used as a template for cutting. 1 mm x 0.12 mm CFRP bands are used as stiffeners. The placement of stiffeners, the overall shape, the wing length, the surface, the aspect ratio or the angle between the sleeves were optimized through experiments.

3 Control mechanism

The control mechanism is the second, but equally important part of the hummingbird prototype. Its role is to generate moments for attitude stabilization and flight control. In our previous work [12] we presented a concept inspired by the Nano hummingbird [10] that produces the moments by modulating the wing twist. This concept, however, requires specific wing design. The produced lift must increase when the membrane is stretched (the twist decreased) and decrease when the the membrane is loosened (the twist increased). Thus, at nominal conditions the wing needs to be operated below its maximal lift.

The alternative concept presented here generates the control moments by modulating the flapping amplitude and offset (mean wing position). Compared to wing twist modulation it is more intuitive and works with any wing design.

3.1 Amplitude and offset modulation via joint displacement

Stabilizing moments can be generated by amplitude and offset modulation as in Figure 1. The roll moment is produced simply by increasing the amplitude of one wing and decreasing the amplitude of the other wing. Moving the mean wing position of both wings forwards or backwards results in a nose-up or nose-down pitch moment, respectively. Finally the yaw moment can be generated by changing the mean wing position asymmetrically.

We have found that both amplitude and offset can be controlled by displacing the mechanism joints marked in Figure 6 a) with orange arrows. The maps in Figure 6 b) show the relation between the position of the joints and the wing amplitude Φ and offset ϕ_0. The blue lines connect positions with constant amplitude and the red lines connect positions

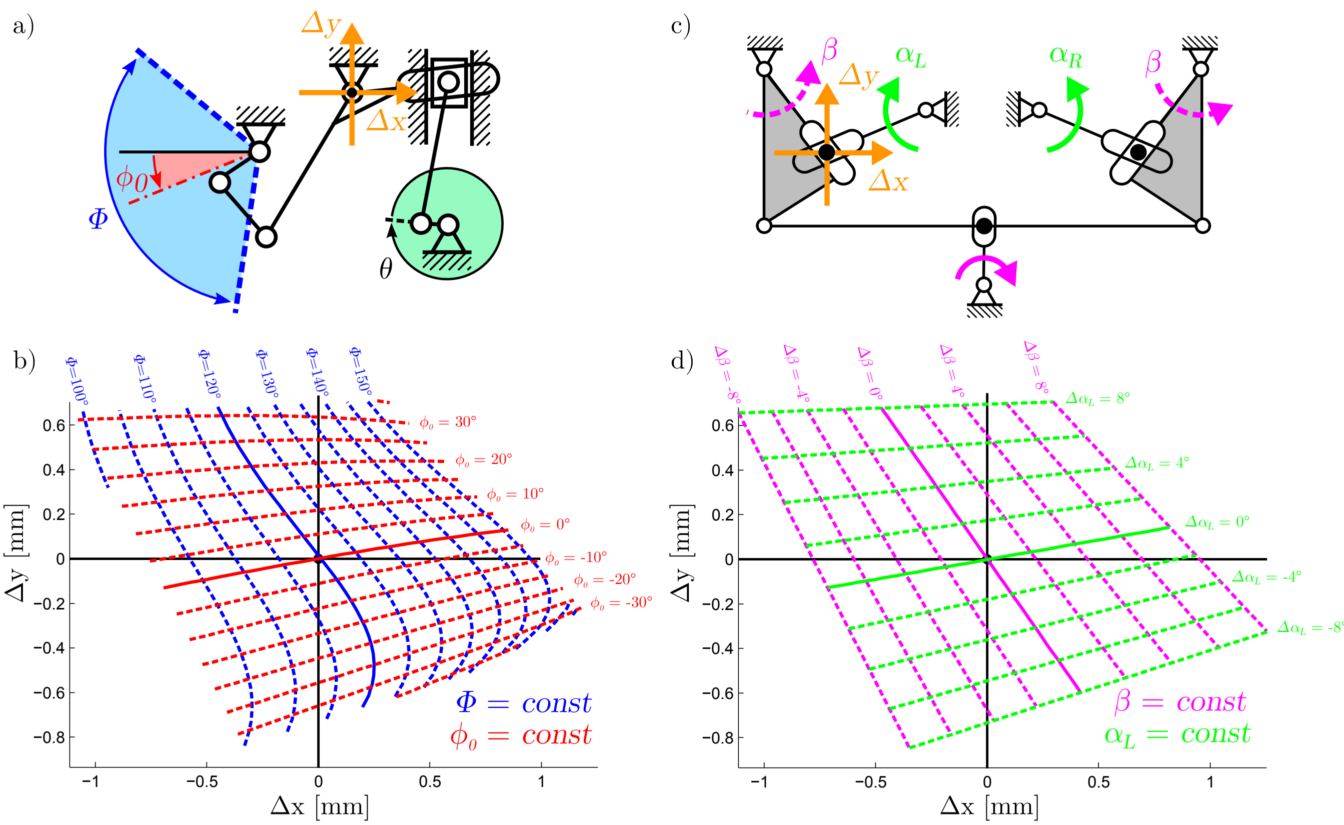

Figure 6: Amplitude and offset modulation via joint displacements: a) the flapping mechanism and its joint displaced by $[\Delta x, \Delta y]$, b) lines of constant amplitude Φ and offset ϕ_0 for varying joint position, c) the control mechanism with 3DOF (α_L, α_R, β) defining the joint position by an intersection of two channels , d) the lines of constant commands α_L and β that approximate well the lines of constant amplitude and offset. Only the plots for the left wing are displayed, the line plots for the right wing are the same but mirrored.

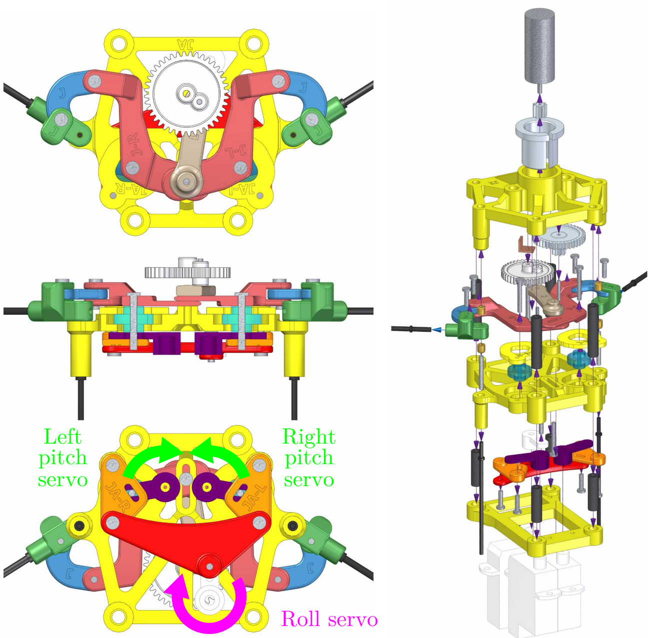

Figure 7: Control mechanism: bottom (left), section (right) and top view on the flapping mechanism with the joint displacement system.

with constant offset. Thus, moving the joint along a blue line will modify the offset, but the amplitude will remain constant. Similarly a displacement along a red line will only affect the amplitude.

It can be noticed that the two sets of curves cross each other at high angles (above 70°) which means the two values can be controlled independently. Moreover, the lines of constant offset are almost straight and nearly parallel; the curves of constant amplitude are also equally spaced and can be approximated by straight lines around the nominal position. This allows to design a joint displacement mechanism with two degrees of freedom (DOF) where the control is decoupled - one DOF controls directly the amplitude and the other controls the offset.

3.2 Control mechanism prototype

The scheme of the proposed mechanism for joint displacement is in Figure 6 c). Each joint is displaced by two links with slots that rotate with respect to the frame by angles α and β, respectively. The joint position is defined by an intersection of the two slots. The link hinges are located on the lines of nominal amplitude and of the nominal offset, respectively. If one of the links is blocked and the other one is moving, the joint moves along a line defined by the slot of the blocked link. If the hinges are placed far enough from the nominal position of the displaced joint ($\Delta x = 0$, $\Delta y = 0$), these lines appear nearly parallel in the region of interest and the joint paths approximate well the theoretical curves of constant amplitude and offset Figure 6 d).

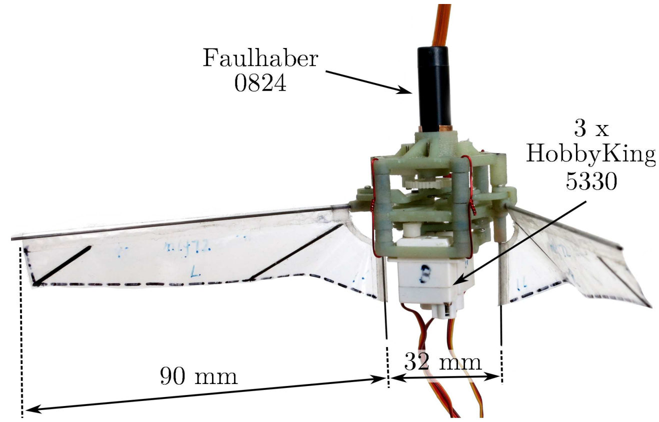

Figure 8: The assembled prototype.

The control of left and right wing offset needs to be independent, operated by separate actuators: a symmetric offset change ($\Delta\alpha_L = \Delta\alpha_R$) will produce pitch moment while asymmetric change ($\Delta\alpha_L = -\Delta\alpha_R$) will produce yaw moment. However, the amplitude can be controlled by a single actuator (β): only asymmetric amplitude changes are needed for roll. This can be achieved by a parallelogram linking the two links responsible for amplitude control (Figure 6 c)).

The final mechanical solution of the joint displacement mechanism is in Figure 7. The rivets of the joints to be displaced are fixed from the top to "anchors" that are free to slide in the horizontal plane of the frame. The displacement is limited to the zone considered in Figure 6 d) by the shape of the frame cut-out. All the parts were 3D printed, a photograph of an assembled prototype is in Figure 8. The mechanism is actuated by three micro servos (HobbyKing 5330) with a weight of 2 g each. The total weight of the controlled prototype including the servos (6 g) and the propulsion motor (5.2 g) is 21.4 g.

4 Experiments

The experiments presented here include high speed camera measurements of the wing kinematics as well as lift and pitch moment measurements on a custom build force balance [12]. Unless mentioned otherwise, all the tests were carried out at a moderate flapping frequency of 15Hz in order to have consistent results in all the tests. For higher frequencies the prototype performance can slightly deteriorate over time due to wear.

4.1 Wing kinematics

To test the function of the control mechanism we used a Photron FASTCAM SA3 high speed camera (resolution 1024 x 1024 pixels). We recorded the prototype wing motion at 500 fps under different control commands and we tracked the sweep angle ϕ at the wing tips according to Figure 9. The amplitude was subsequently calculated as $\Phi = \phi_{max} - \phi_{min}$

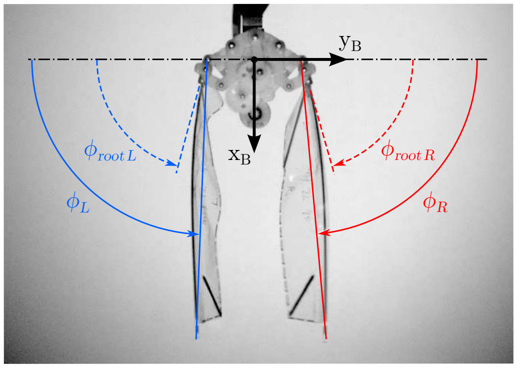

Figure 9: Definition of the tracked angles.

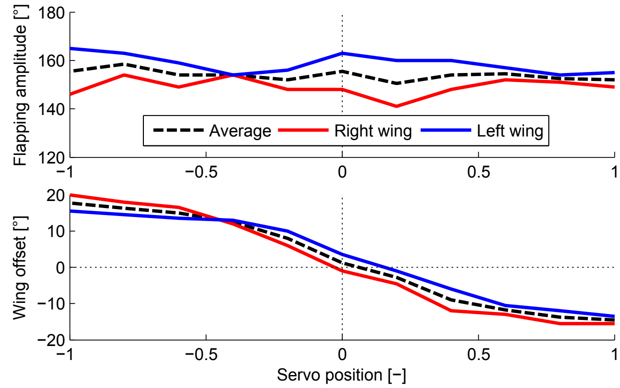

Figure 11: Offset control with the pair of pitch servos.

and offset as $\phi_0 = (\phi_{max} + \phi_{min})/2$, where ϕ_{max} and ϕ_{min} are the maximal and minimal observed angles ϕ, respectively. The observed amplitudes were much larger than the design value of 120° due to compliance of the wing bars and partly also due to mechanism backlash.

Figure 10 shows the results of amplitude difference control. The servos controlling the wing offset were kept in their nominal position and the roll control servo was commanded from the minimal to the maximal position with a step of 10% of the full range. The left and right wing amplitudes, Φ_L and Φ_R, are approximately equal for zero servo position. As intended, their difference $\Delta\Phi = \Phi_R - \Phi_L$ increases/decreases approximately linearly as the servo moves towards the positive/negative limit, where the difference is $+52°$ and $-44°$, respectively. Thus, a good control authority of the roll moment is achieved. The wing offset remains relatively close to zero and the average amplitude $\bar{\Phi} = (\Phi_R + \Phi_L)/2$ stays approximately constant (around 155°) in the central part of the servo range. There exist some imperfections, in particular close to the limits, but these should be compensated by feedback control in future.

The offset control is presented in Figure 11. The left and right offset servos were commanded together over the full range, again with a step of 10%. The roll servo was kept at zero. We again see a good control authority over the wing offset, being linear around the origin with a slight decrease of slope closer to the limits. The maximal and minimal average offset $\bar{\phi}_0 = (\phi_{0R} + \phi_{0L})/2$ is $+17.7°$ and $-14.5°$, respectively. The amplitude of the left and right wing varies quite a lot, but the average $\bar{\Phi}$ stays close to 155°. A simultaneous control of the amplitude difference would be necessary to achieve zero roll moment. We will discuss the combined commands and resulting coupling effects at the end of this section.

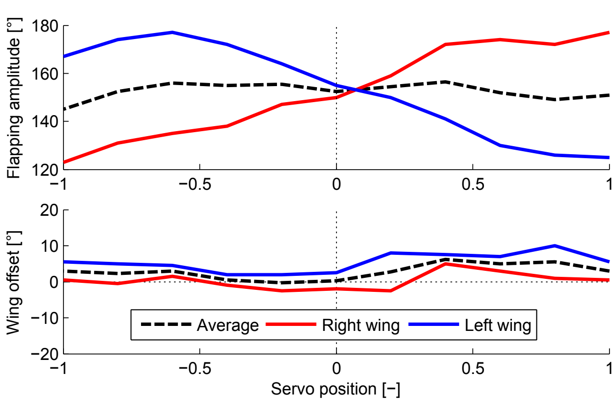

Figure 10: Amplitude control with the roll servo.

4.2 Control mechanism dynamics

Figures 12 and 13 show the dynamics of the transition from minimal to maximal command of pitch and roll, respectively. For this experiment the flapping frequency was 17Hz. The figures display the wing tip angles, their extremal positions are connected with a dashed line and the average position (over the last wingbeat) is displayed as dash-dotted line. An LED was placed on the prototype to indicate the moment of the step command (black line).

As can be seen in Figure 12 the transition from maximal to minimal offset occurs within 2 wingbeats. The transition from negative to positive amplitude difference takes around 4 wingbeats (Figure 13), however an opposite sign of the difference is achieved already for 2 wingbeats. The same could be observed for the step commands in opposite directions.

We have two explanations for the faster pitch command. First, in offset control two servos are employed, one acting on each joint, while in the roll command only a single servo is displacing the two joints. The second reason is that the reaction due to the flapping motion on the displaced joints has a major component in the direction, where the joints are displaced for offset control. This speeds up the offset transition when a change is desired, but has an adverse effect on the mechanism efficiency as the joints keep shaking in this direction during operation.

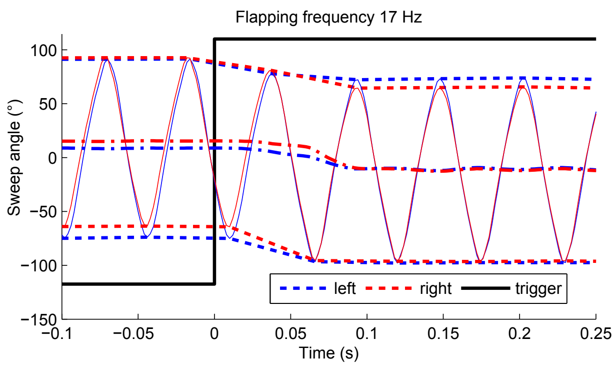

Figure 12: Pitch up → down command dynamics

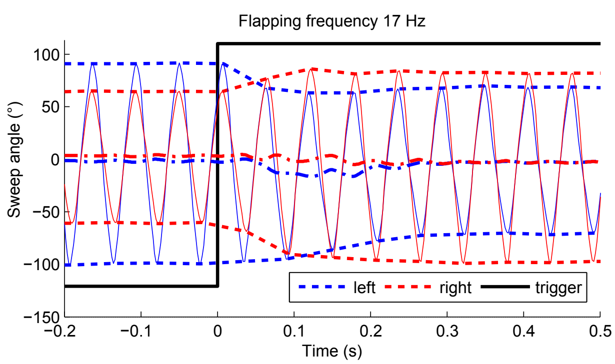

Figure 13: Roll left → right command dynamics

4.3 *Pitch moment and lift generation*

Apart from wing kinematics measurements the performance of the prototype was tested directly on a force balance. The custom built balance was presented in [12]. It was designed to measure cycle averaged lift and pitch moment with a help of two double cantilever beams with strain gages.

Figure 14 shows the measured pitch moment, lift, frequency and motor current as a function of the offset servos position. We kept the motor voltage at 4.2V, at which the flapping frequency is approximately 15Hz for the nominal servo position. The measured pitch moment ranged from -0.5 N.mm to 0.8 N.mm. The lift force and frequency increase and the current decreases when the servos approach the limit positions. This is caused by the shaking of the displaced joints due to flapping (already mentioned earlier) that happens particularly for the central servo positions. The joints get a better fix in the limit positions, where the servo pushes the displaced joints against a wall of the frame, and thus the efficiency increases. The lift varies between 53 and 59 mN and the frequency between 14.9 and 16.2 Hz, which fits the lift vs frequency characteristic of the uncontrolled prototype (joints are fixed). However, the electrical power of the controlled version is almost twice as high due to losses in the shaking joints.

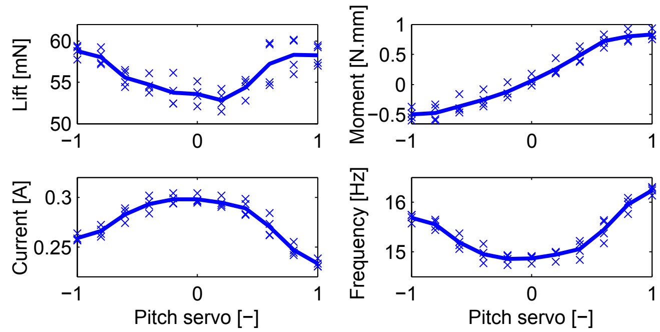

Figure 14: Lift, pitch moment, motor current and flapping frequency against pitch servos position. Measurement done at 15 Hz, individual measurements are displayed as crosses, the solid line represents an average of four measurements.

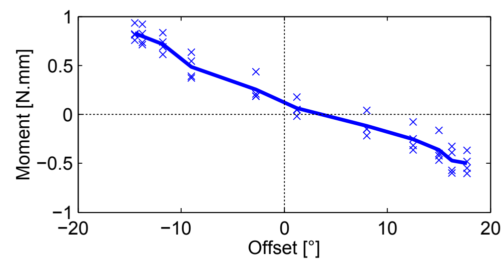

Figure 15: Pitch moment against wing offset.

In Figure 15 we combine the wing kinematics measurement from the previous part with the moment measurement. The relationship is approximately linear with a slope of 0.04 N.mm per degree. The non-zero moment produced at zero offset can be explained by a combination of asymmetric wing design (stiffeners glued only from one side), different velocity profiles in upstroke and downstroke and by an imperfect alignment of the prototype on the balance. Nevertheless, a compensating moment can be easily introduced by an offset of the COG from the shoulders in the longitudinal direction.

Figure 16 shows the pitch moment, lift, frequency and motor current for motor voltages up to 6V. We plot three curves for pitch servos at positions -1, 0 and 1, related to the full range. The behaviour corresponds to the one observed at 15Hz. At the highest tested voltage the mechanism produces pitch moments from -0.7 N.mm to 1.1 N.mm while the lift ranges between 90 and 100 mN.

4.4 *Combined commands*

Finally, we tested combinations of pitch and roll commands to identify the amount of cross-coupling. Again all the measurements were carried out at a constant motor voltage (4.2V) giving a flapping frequency of around 15Hz at the nominal servos position. The measurements were taken at servo positions -0.8, -0.4, 0, 0.4 and 0.8 of the full range for both pitch and roll servos. Thus, 25 measurements were taken in total.

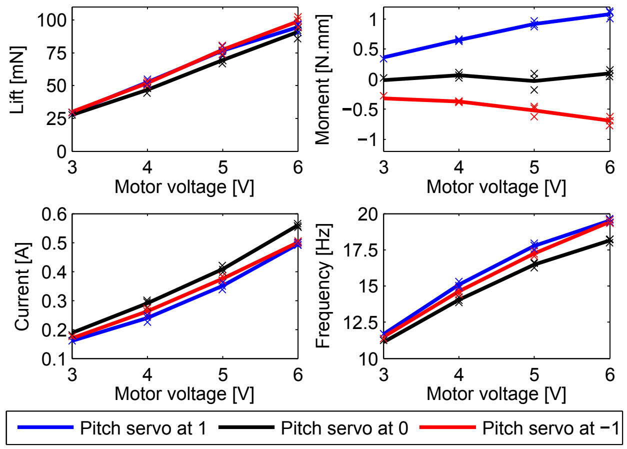

Figure 16: Lift, pitch moment, motor current and flapping frequency measured for increasing motor voltage. Black lines represent the zero pitch servos position, red and blue lines represent the minimal and maximal pitch command. The crosses represent individual measurements.

Figure 17 shows the amplitude and offset maps of the left and the right wing as obtained from the high speed recordings. We can see that while small cross-coupling always exists, moving the roll servo has a dominant effect on the amplitude and the pitch servo has a dominant effect on the offset. Moreover, the relation between the amplitude/offset and roll/pitch servo positions stays always monotonic. Thus, a feedback controller should be able to compensate the coupling effects and the small differences between left and right wing behaviour, caused by the mechanism imperfections.

The same experiment was repeated with the force balance, the results are in Figure 18. The maps show the pitch moment and lift force maps for the servo input combinations considered. The lift map keeps a valley-like shape in the pitch servo direction, similar to what was observed for the pure pitch command and what can be explained by improper joint fixation in the central pitch servo positions. There is also a smaller increase of lift in the positive roll direction, which we believe comes from the imperfections of the prototype. The minimum and maximum lift is 48 and 59 mN, respectively. The lift force variation is related to the square of the frequency times amplitude in Figure 17 c).

The pitch moment depends mostly on pitch servo positions, while there are only minor differences when the roll servo position changes. Thus, the minimal and maximal pitch values stay at the same levels as for the pure pitch command, -0.4 N.mm and 0.8 N.mm respectively. The pitch moment corresponds closely to the mean offset in Figure 17 f).

5 Conclusion

We presented a control mechanism for a flapping wing MAV that generates necessary control moments by modulating the flapping wing amplitude and offset. A novel concept of joint displacement is used to modify the kinematics of the linkage mechanism producing the flapping motion. We demonstrated experimentally that sufficient offset ($\pm 15°$) and amplitude differences (above $\pm 40°$) for pitch and roll control can be introduced by very small displacements of the linkage joints (below $\pm 1mm$) in two directions. The transitions between maximum and minimum command takes two wingbeats in pitch and up-to four wingbeats in roll. Moreover, very low level of cross-coupling exists for combined commands. The prototype can produce pitch moments between -0.7 N.mm and 1.1 N.mm while flapping at frequencies around 18Hz and producing a lift of at least 90mN.

While the control mechanism succeeds in modifying the wing kinematics, the prototype efficiency drops significantly compared to the uncontrolled prototype. The drawback of the proposed solution is that the displaced joints need to hold rather large and oscillating reaction forces due to flapping. This causes the joints to shake, which reduces significantly the mechanism performance and at higher frequencies also its lifespan. The motor draws up to twice the electrical power compared to an uncontrolled prototype with fixed joints. We are working on an alternative mechanical solution that should reduce the effect of the oscillating reaction on the servos displacing the joints.

Acknowledgements

The research of M. Karásek was supported by FRIA fellowship from F.R.S.-FNRS in Belgium (FC 89554).

References

[1] G. K. Taylor and A. L. R. Thomas. Dynamic flight stability in the desert locust schistocerca gregaria. *Journal of Experimental Biology*, 206(16):2803–2829, Aug. 2003.

[2] M. Sun and Y. Xiong. Dynamic flight stability of a hovering bumblebee. *Journal of Experimental Biology*, 208:447–459, 2005.

[3] C. T. Orlowski and A. R. Girard. Dynamics, stability, and control analyses of flapping wing micro-air vehicles. *Progress in Aerospace Sciences*, 51:18–30, 2012.

[4] M. Karasek and A. Preumont. Flapping flight stability in hover: A comparison of various aerodynamic models. *International Journal of Micro Air Vehicles*, 4(3):203–226, 2012.

[5] C. P. Ellington. The novel aerodynamics of insect flight: application to micro-air vehicles. *Journal of Experimental Biology*, 202:3439–3448, 1999.

[6] L. Ristroph, G. Ristroph, S. Morozova, A. J. Bergou, S. Chang, J. Guckenheimer, Z. J. Wang, and I. Cohen. Active and passive stabilization of body pitch in insect flight. *Journal of The Royal Society Interface*, 10(85):1–13, 2013.

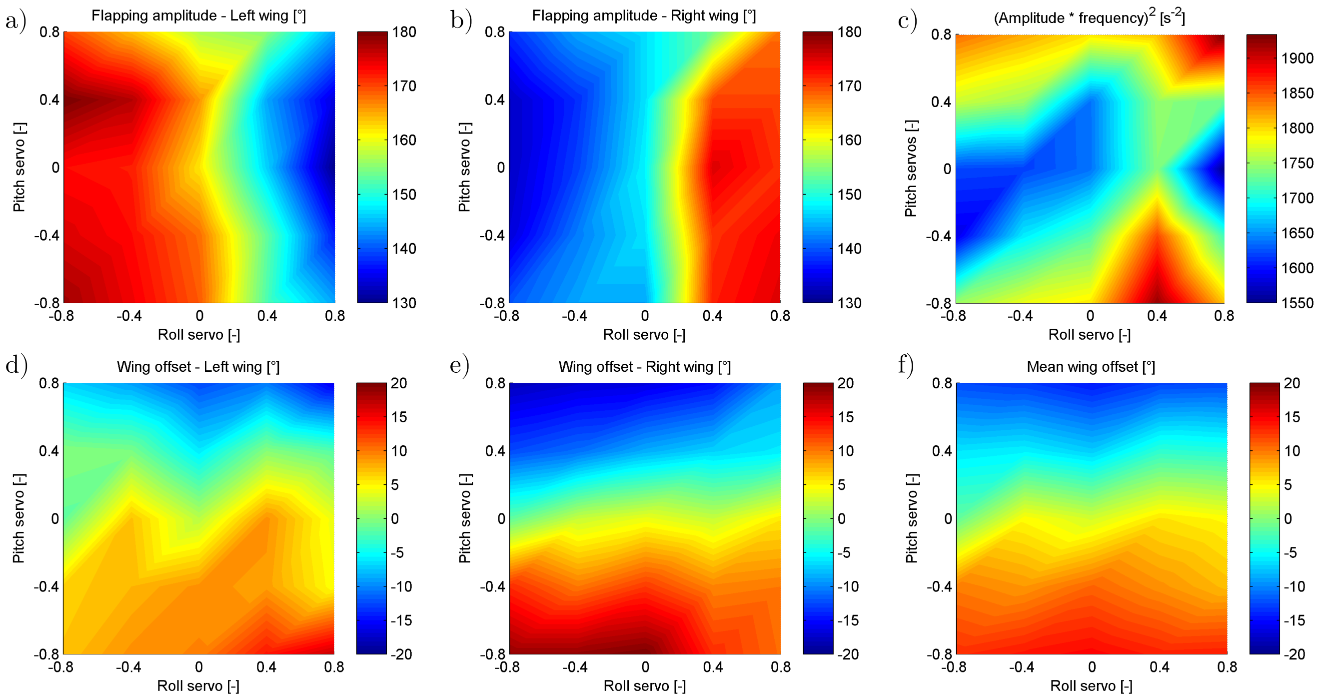

Figure 17: Kinematics measurements for combined pitch and roll servo commands: a) left amplitude, b) right amplitude, c) square of mean amplitude times frequency, d) left offset, e) right offset, f) mean offset.

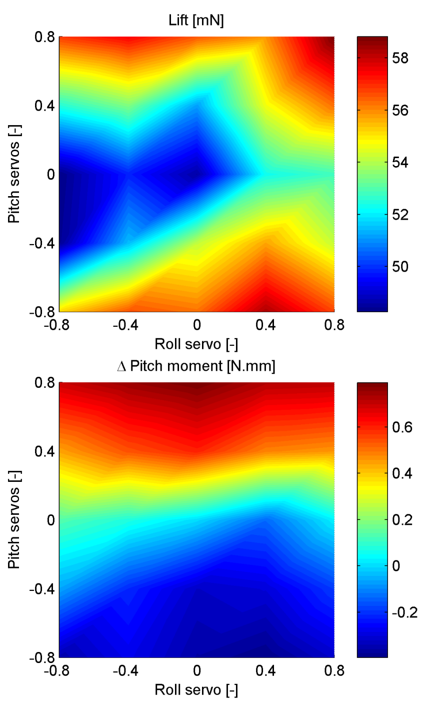

Figure 18: Force balance measurements for combined pitch and roll servo commands: lift (top) and pitch moment (bottom). Lift is tied to the square of mean amplitude times frequency (Figure 17 c)) and moment corresponds to the mean offset (Figure 17 f)).

[7] G.C.H.E. de Croon, K.M.E. de Clerq, R. Ruijsink, B. Remes, and C. de Wagter. Design, aerodynamics, and vision-based control of the delfly. *International Journal of Micro Air Vehicles*, 1(2):71–97, Jun. 2009.

[8] F. van Breugel, Z. E. Teoh, and H. Lipson. A passively stable hovering flapping micro-air vehicle. In D. Floreano, J.-C. Zufferey, M. V. Srinivasan, and C. P. Ellington, editors, *Flying Insects and Robots*, pages 171–184. Springer Berlin Heidelberg, 2010.

[9] C. Richter and H. Lipson. Untethered hovering flapping flight of a 3d-printed mechanical insect. *Artificial life*, 17(2):73–86, 2011.

[10] M. Keennon, K. Klingebiel, H. Won, and A. Andriukov. Development of the nano hummingbird: A tailless flapping wing micro air vehicle. *AIAA paper 2012-0588*, pages 1–24, 2012.

[11] K. Y. Ma, P. Chirarattananon, S. B. Fuller, and R. J. Wood. Controlled flight of a biologically inspired, insect-scale robot. *Science*, 340:603–607, 2013.

[12] M. Karasek, Y. Nan, I. Romanescu, and A. Preumont. Pitch moment generation and measurement in a robotic hummingbird. *International Journal of Micro Air Vehicles*, 5(4):299–309, 2013.